Supporting Information

Contrasting Efficiency of Electron-induced Reaction at Cu(110) in Aliphatic and Aromatic Bromides

Matthew J. Timm[1], Lydie Leung[1], Kelvin Anggara[1], Tingbin Lim[1], Zhixin Hu[1], Simone Latini[2], Angel Rubio[2] and John C. Polanyi[1*]

[1]*Lash Miller Chemical Laboratories, Department of Chemistry and Institute of Optical Sciences, University of Toronto, 80 St. George Street, Toronto, Ontario, M5H 3H6, Canada*
[2]*Max Planck Institute for the Structure and Dynamics of Matter, Luruper Chaussee 149, 22761 Hamburg, Germany*
Center for Free-Electron Laser Science and Department of Physics, University of Hamburg, Luruper Chaussee 149, 22761 Hamburg, Germany

Corresponding author: john.polanyi@utoronto.ca

1. Materials and Methods

Experiment

Experiments were carried out using a low-temperature Scanning Tunneling Microscope (Omicron) in an ultra-high vacuum chamber with a base pressure $< 3 \times 10^{-11}$ mbar. The Cu surface was prepared by repeated cycles of Ar^+ sputtering (0.6 keV, 7 μA) and annealing (800 K) until less than 1% of contaminants were detected by STM. Tungsten STM tips were made by a 4.5-9 V direct-current etch in 3 M NaOH solution.

Both compounds in this study, pentyl bromide (1-bromopentane ≥ 99%) and phenyl bromide (1-bromobenzene ≥ 99%) were purchased from Sigma-Aldrich and were colorless liquids. Prior to dosing both compounds were purified by multiple cycles of freeze-pump-thaw. Each compound was dosed through a capillary tube directed towards the Cu surface with the sample reaching a maximum temperature of 12.6 K during the dose. All images were recorded in constant-current mode at a temperature of 4.6 K.

C-Br bond dissociation was performed by placing the tip over the center of the reagent, either pentyl bromide (PeBr) or phenyl bromide (PhBr), and recording the current versus time at a constant bias with the feedback loop turned off for up to 5 seconds. The bias used to induce

dissociation was 2.1 eV for PeBr and 2.0 eV for PhBr, with the bias given with respect to the sample. These bias values were above the energy-threshold for dissociation. They promoted dissociation in preference to diffusion, at lower biases. A reactive event was signaled by a single abrupt discontinuity in the recorded current. Only cases that gave a single discontinuity were considered. The occurrence of reaction was confirmed by imaging the reaction products in the subsequent scan. The product positions, with respect to the center of the physisorbed reagent, were analyzed using WSxM software.[1]

Theory

Density Functional Theory (DFT) calculations were performed using the Vienna Ab initio Simulation Package (VASP)[2,3] on the SciNet supercomputer,[4] the Niagara cluster,[5] in order to model the experimental results. Calculations used the projector augmented wave (PAW) method[6,7] and the generalized gradient approximation (GGA) with the Predew-Burke-Ernzerhof (PBE) functional.[8] Grimme's semi-empirical dispersion correction (DFT-D3) was added to correct for Van der Waals interactions.[9] The cut-off energy for the plane-wave basis set was 400 eV.

The Cu(110) surface was modelled using a periodically repeated slab model. The (4 × 6) supercell consisted of 120 Cu-atoms in five atomic layers, plus the adsorbed molecule and a vacuum region of at least 17 Å. All atoms were allowed to relax until the force on each atom was less than 0.01 eV $Å^{-1}$, except for the lowest Cu-atom layer which was frozen at the theoretically optimized Cu lattice constant of 3.5673 Å. A single Γ-point *k*-mesh was used for structural optimizations, STM-simulations, atomic orbital projected density-of-states (pDOS) calculations with Gaussian smearing of σ = 0.25 eV, and molecular dynamics (MD) calculations. A denser *k*-mesh (3 × 3 × 1) was used to evaluate adsorption energies. Molecular structures were visualized using the Visual Molecular Dynamics (VMD) software.[10,11] STM simulations were performed using the Tersoff-Hamann approximation[12] and were visualized using the Hive Software.[13,14]

The MD calculations using the impulsive-two-state (I2S) model, were performed to simulate the electron-induced dissociation of PeBr and PhBr. This model utilizes an ionic pseudopotential method[15,16] to obtain the intramolecular repulsion due to electron attachment. To construct the repulsive anionic potential-energy surface (pes*) a single 3d electron from the Br-atom core was promoted to the Br atom's valence shell to generate the electronic configuration $[Ar]4s^2 3d^9 4p^6$. The system was then evolved on the repulsive pes* for a short period of time (t* = 50fs for PeBr, t* = 40 fs for PhBr) before being returned to the neutral ground state potential

energy surface (pes) with a retention of the positions and momenta obtained while on the pes*. The system was allowed to evolve until chemisorbed reaction products were formed. The MD calculations were carried out under the microcanonical condition, with a time step of 0.5 fs in order to give a negligible energy drift (< 4 meV ps^{-1}).

The calculations for the projected density of states of the adsorbed molecules onto the gas phase molecular orbitals have been performed with the GPAW code.[17,18] As in the case of VASP, the calculations were based on the PAW method and made use of the PBE density functional. The same geometry, supercell size, cutoff energy and k-point sampling (Γ-point *k*-mesh) has been adopted.

The molecular orbital resolved projected density of states has been obtained for the both PeBr and PhBr according to the following equation:

$$\rho_{\tilde{n}}(E) = \sum_n |< \phi_{\tilde{n}} | \psi_n >|^2 \delta(E - E_n) \,,$$

where $\phi_{\tilde{n}}$ is the molecular orbital $\tilde{n}$ of the molecule in gaseous phase with a frozen geometry corresponding to the adsorbed phase (as shown in Figure S3) and ψ_n the wavefunction n of the molecule plus Cu-surface system. The Dirac delta in the equation above has been approximated with a Lorentzian with an artificial width of 0.15 eV.

2. Molecular adsorption of pentyl bromide (PeBr) and phenyl bromide (PhBr) on Cu(110) at 4.6 K.

Figure S1 gives an example of an STM image obtained after deposition of pentyl bromide and phenyl bromide molecules at 12.6 K, recorded at 4.6 K. For the case of the pentyl bromide adsorbed on Cu surface, several features are observed. Isolated single PeBr molecules are found with two orientations as shown in the insets of Figure S1A. A major orientation (77 ± 5 %) with the PeBr molecular axis was observed at an angle from the [001] direction and a minor orientation (23 ± 2 %) with the molecular axis parallel to the $[1\bar{1}0]$ direction. The other features observed were PeBr aggregates. PhBr was observed as isolated intact molecules on Cu(110) as shown in Figure S1B. Its molecular axis was found at an angle (26º) from the [001] direction as displayed in the inset of Figure S1B.

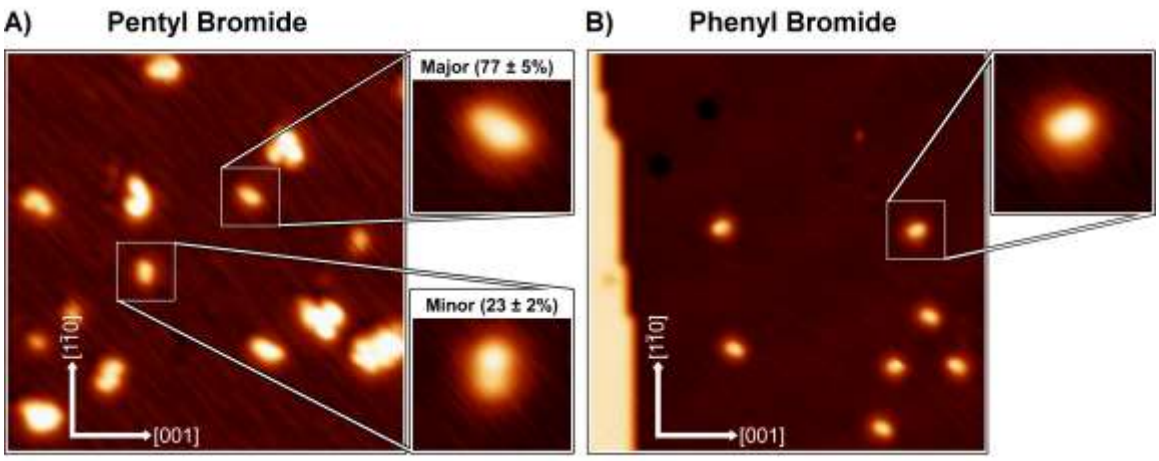

Figure S1. Large scale STM images of (A) PeBr (20 × 20 nm^2, *I*= 0.01 nA and *V*= –0.05 V) and (B) PhBr (20 × 20 nm^2, *I*= 0.20 nA and *V*= 0.05 V) adsorbed on Cu(110) at 4.6 K. The configurations of the isolated molecules are displayed in the insets (STM images for PeBr: 3 × 3 nm^2, *I*= 0.01 nA and *V*= –0.05 V, and STM image for PhBr: 3 × 3 nm^2, *I*= 0.10 nA and *V*= 0.015 V).

3. Comparison of Pe and Br distributions obtained from the electron-induced reaction of PeBr for the major and minor configurations.

Figure S2 shows the angular and distance distribution for the products of the induced dissociation of PeBr. For both configurations, the Br-atom and pentyl recoiled in opposite directions along the C-Br bond. The adsorption geometry of the major PeBr configuration is presented in Figure S2A and consists of the hydrocarbon chain lying parallel to the Cu surface, along the [1$\bar{1}\bar{1}$] direction. The minor adsorption geometry is shown in Figure S2B, with its hydrocarbon chain lying parallel to the surface, along the [1$\bar{1}$0] direction. The product distribution originating from the two configurations were similar, with the pentyl found mainly in the lower left (backward) hemisphere and the majority of Br-atoms observed in the right (forward) hemisphere along the [001] direction.

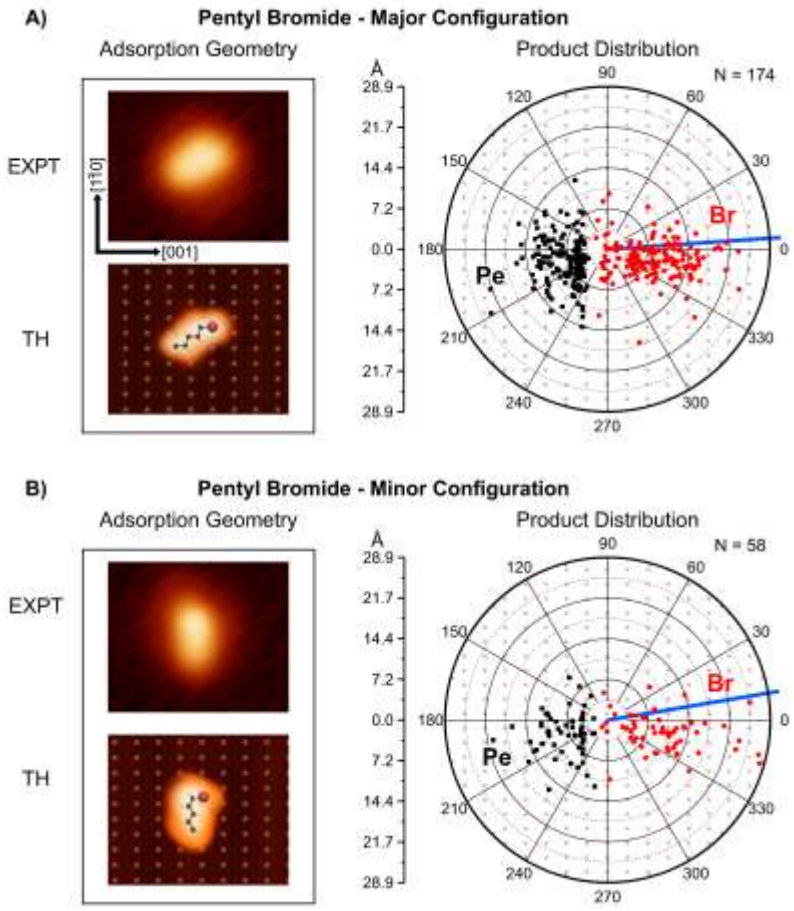

Figure S2. Comparison of the adsorption (at left) and product (at right) distribution for PeBr adsorbed on Cu(110) at 4.6 K, (A) major parent and (B) minor parent configurations. The reagent configuration was folded to a single representative configuration corresponding to the adsorption geometry. The origin of both plots is the Br-atom in the reagent. The blue line indicates the prior C-Br bond direction. The black squares indicate the position of the scattered pentyl, whereas the red dots indicate that of the Br-atom. The Cu surface is underlaid, with the circles one unit cell (3.61 Å) apart.

4. Gas-phase molecular orbitals for PeBr and PhBr.

The C-Br σ* anti-bonding orbital was assigned to the LUMO for PeBr and LUMO+2 for PhBr by comparison with the gas-phase molecular orbitals calculated for the frozen adsorption configurations of PeBr and PhBr on the Cu surface, as shown in Figure S3.

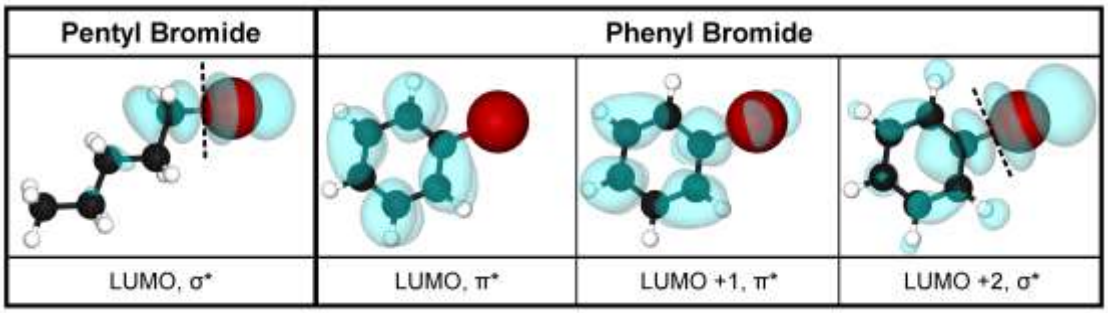

Figure S3. Gas-phase molecular orbitals frozen at the adsorption configurations computed for the PeBr and PhBr. The dashed line indicates the nodal plane of the C-Br σ* anti-bonding orbital.

5. Comparison of the product-distributions obtained after electron-induced dissociation of PhBr for two reaction pathways; typical and 'rotated'.

For the case of the PhBr electron-induced dissociation, a secondary product distribution was observable comprising 27 ± 3 % of the total, in addition to the primary distribution shown in Figure 2B of the main text; this minor contribution is displayed in Figure S4B. Since the phenyl and Br-atom products recoiled in opposite directions, the minor distribution indicated that a fraction of the reagent had rotated around its centre-of-mass during dissociation. The products of this secondary distribution were found primarily in the upper backward hemisphere for the phenyl radical, and therefore in the lower forward hemisphere for the Br-atom. This constitutes a rotated configuration for the minor 27% of the Br, as shown in Figure S4B, resulting from a C-Br bond which has rotated by – 52° from its original direction.

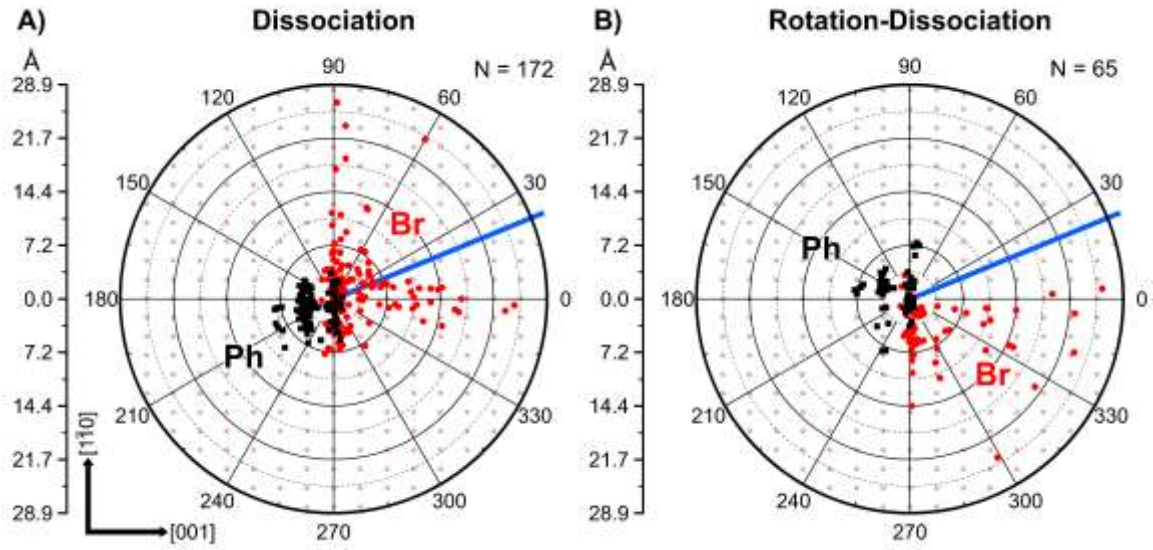

Figure S4. Comparison of the distance and angle distributions of the products for PhBr following (A) the major pathway (73%) for induced dissociation and (B) the minor pathway (27%), the latter appearing to result from rotation of the molecule during dissociation. The reagent PhBr configuration was folded to a single representative configuration in (B). The origin of both plots is the Br-atom in PhBr. The blue line indicates the original direction of the reagent C-Br bond. The C-Br bond gives evidence of having rotated during dissociation in (B). Black squares indicate the position of the phenyl radical; red dots the position of the Br-atom. The Cu surface is underlaid with circles one unit cell (3.61 Å) apart.

6. References

1. Horcas, I.; Fernández, R.; Gómez-Rodríguez, J. M.; Colchero, J.; Gómez-Herrero, J.; Baro, A. M. WSXM: A software for scanning probe microscopy and a tool for nanotechnology. *Rev. Sci. Instrum.* **2007**, *78*, 013705.
2. Kresse, G.; Hafner, J. Ab initio molecular dynamics for liquid metals. *Phys. Rev. B* **1993**, *47*, 558–561.
3. Kresse, G.; Furthmüller, J. Efficient iterative schemes for ab initio total-energy calculations using a plane-wave basis set. *Phys. Rev. B* **1996**, *54*, 11169–11186.
4. Loken, C.; Gruner, D.; Groer , L.; Peltier, R.; Bunn, N.; Craig, M.; Henriques, T.; Dempsey, J.; Yu, C.-H.; Chen, J.; Dursi, J. L.; Chong, J.; Northrup, S.; Pinto, J.; Knecht, N.; van Zon, R. SciNet: Lessons learned from building a power-efficient top-20 system and data centre. *J. Phys. Conf. Ser.* **2010**, *256*, 12026.
5. Ponce, M.; van Zon, R.; Northrup, S.; Gruner, D.; Chen, J.; Ertinaz, F.; Fedoseev, A.; Groer, L.; Mao, F.; Mundim, B. C.; Nolta, M.; Pinto, J.; Saldarriaga, M.; Slavnic, V.; Spence, E.; Yu, C.-H.; Peltier, W. R. Deploying a Top-100 Supercomputer for Large Parallel

Workloads: the Niagara Supercomputer. In Proceedings of the Practice and Experience in Advanced Research Computing on Rise of the Machines (learning) (PEARC '19). Association for Computing Machinery, New York, NY, USA, **2019**, Article 34, 1–8.

6. Blöchl, P. E. Projector augmented-wave method. *Phys. Rev. B* **1994**, *50*, 17953–17979.
7. Kresse, G.; Joubert, D. From ultrasoft pseudopotentials to the projector augmented-wave method. *Phys. Rev. B* **1999**, *59*, 1758–1775.
8. Perdew, J. P.; Burke, K.; Ernzerhof, M. Generalized gradient approximation made simple. *Phys. Rev. Lett.* **1996**, *77*, 3865–3868.
9. Grimme, S.; Antony, J.; Ehrlich, S.; Krieg, H. A consistent and accurate ab initio parametrization of density functional dispersion correction (DFT-D) for the 94 elements H-Pu. *J. Chem. Phys.* **2010**, *132*, 154104.
10. Humphrey, W.; Dalke, A.; Schulten, K. VMD - Visual Molecular Dynamics, *J. Molec. Graphics* **1996**, *14*, 33-38.
11. http://www.ks.uiuc.edu/Research/vmd/
12. Tersoff, J.; Hamann, D. R. Theory of the scanning tunneling microscope. *Phys. Rev. B* **1985**, *31*, 805–813.
13. Vanpoucke, D. E. P.; Brocks, G. Formation of Pt-induced Ge atomic nanowires on Pt/Ge(001): A density functional theory study. *Phys. Rev. B* **2008**, *77*, 241308.
14. Vanpoucke, D. E. P. Ab initio study of Pt Induced Nanowires on Ge(001), Ph.D. Thesis at University of Twente, The Netherlands **(2009).**
15. Joubert, D.; Kresse, G. From ultrasoft pseudopotentials to the projector augmented-wave method. *Phys. Rev. B* **1999**, *59*, 1758-1775.
16. Kohler, L.; Kresse, G. Density functional study of CO on Rh(111). *Phys. Rev. B* **2004**, *70*, 165405.
17. Mortensen, J. J.; Hansen, L. B.; Jacobsen, K. W. Real-space grid implementation of the projector augmented wave method. *Phys. Rev. B* **2005**, *71*, 035109.
18. Enkovaara, J.; Rostgaard, C.; Mortensen, J. J.; Chen, J.; Dułak, M.; Ferrighi, L.; Gavnholt, J.; Glinsvad, C.; Haikola, V.; Hansen, H. A.; et al. Electronic structure calculations with GPAW: a real-space implementation of the projector augmented-wave method. *J. Phys.: Condens. Matter* **2010**, *22*, 253202.